Length Dependence of Charge Transport in Nanoscopic Molecular Junctions Incorporating a Series of Rigid Thiol-Terminated Norbornylogs

Jeremy M. Beebe,[†] Vincent B. Engelkes,[‡] Jingquan Liu,[§] J. Justin Gooding,[§] Paul K. Eggers,[§] Yongseok Jun,[†] Xiaoyang Zhu,[†] Michael N. Paddon-Row,*[,§] and C. Daniel Frisbie*[,‡]

Department of Chemistry, University of Minnesota, 209 Pleasant Street SE, Minneapolis, Minnesota 55455, Department of Chemical Engineering and Materials Science, University of Minnesota, 421 Washington Avenue SE, Minneapolis, Minnesota 55455, and School of Chemistry, University of New South Wales, Sydney, NSW 2052, Australia

Received: November 24, 2004; In Final Form: January 13, 2005

Four tetrathiol-terminated norbornane homologues were synthesized and self-assembled monolayers (SAMs) of these molecules were formed on Au via adsorption from CH_2Cl_2. SAMs were characterized structurally via spectroscopic ellipsometry (SE), reflection−absorption infrared spectroscopy (RAIRS), Rutherford backscattering spectrometry (RBS), and X-ray photoelectron spectroscopy (XPS). Results of these analyses show that the rigid norbornylogs form monolayers that have a surface coverage slightly lower than that of alkanethiols, and that they exhibit a nonmonotonic dependence of film thickness on molecular length. Nanoscale molecular junctions incorporating these SAMs were formed and characterized electrically using conducting probe atomic force microscopy (CP-AFM). The resistances of these junctions scale exponentially with the contour length of the molecules, with $\beta = 0.9$ Å^{-1}, consistent with a nonresonant tunneling mechanism. Further, the resistance of norbornyl SAMs correlates well with the resistance of alkanedithiol SAMs of similar length, suggesting that the norbornyl molecules form sulfur−metal bonds on both ends of the junction.

Introduction

The formation and characterization of metal−molecule−metal junctions is of central importance to molecular electronics. Several strategies exist for probing the electrical characteristics of molecules by sandwiching them between metal electrodes. These methods include break junctions,[1,2] nanopores,[3,4] crossed wires,[5,6] Hg-drop electrodes,[7−10] scanning tunneling microscopy (STM),[11−15] and conducting probe-atomic force microscopy (CP-AFM).[16−20] Already a wide range of electrical transport behaviors have been observed, including negative differential resistance,[14,21,22] rectification,[6,7,23] conductance quantization,[24,25] and switching.[9,26,27] In general, the goal of making conductance measurements on molecules in nanoscale junctions is to examine the effects of structure and electronic properties on the charge transport characteristics of the molecular bridge.

Recently, we have used CP-AFM to make molecular junctions based on self-assembled monolayers of alkanethiols,[28] alkanedithiols,[29] alkyl isocyanides,[30] and oligophenylenethiols.[18] In this technique, SAMs are grown on a metal substrate that is brought into contact with a metal-coated AFM tip under controlled load. Typically, a bias is swept at the tip, and the substrate is held at ground, allowing the current−voltage characteristics of the junction to be measured. At low bias, the current−voltage curves are linear, and the reciprocal of the slope is the low-bias junction resistance. We use CP-AFM in this manner to measure junction resistance as a function of molecular length. The resistance−length characteristic quantifies the efficiency of transport and reflects the transport mechanism (usually nonresonant tunneling in the cases we have examined). We have also shown that the resistance versus length characteristic can be used to provide estimates of contact resistance.[29,30]

Here we report CP-AFM tunneling measurements through self-assembled monolayers of a new series of norbornylogous molecules **1**−**4**, shown in Figure 1. These molecules are long, rigid, and curved. In principle, these characteristics make these molecules good candidates for determining whether transport occurs via a through-bond mechanism, in which charge travels along the contour length of the molecule, or a through-space mechanism, in which charge tunnels in a straight-line path from one electrode to the other. The debate over through-bond or through-space tunneling has occurred repeatedly in chemistry, for example in the discussion of electron transfer in proteins,[31−33] DNA,[34−36] and donor−bridge−acceptor compounds.[37−42] The preponderance of evidence in these systems points to through-bond tunneling as the dominant mechanism. Prior work by one of us involving molecules similar to the norbornylogs used in this study overwhelmingly supports a through-bond tunneling mechanism in solution.[37−42] However, rigid norbornylogs have not yet been exploited as functional components in molecular junctions.

One factor that affects electron transport in the solid state is the arrangement of molecules on the substrate surface. As discussed later, SAMs of the norbornylogs display a nonmonotonic dependence of SAM thickness on the number of carbon atoms in the molecular backbone**.** At first glance, this should provide a pathway for distinguishing between through-bond and through-space charge transport in molecular junctions, because it should be possible to examine whether conductance scales with the number of carbon atoms or with SAM thickness. However, after extensive monolayer characterization, we show that a change in molecular orientation occurs within the SAMs,

[†] Department of Chemistry, University of Minnesota.
[‡] Department of Chemical Engineering and Materials Science, University of Minnesota.
[§] School of Chemistry, University of New South Wales.

10.1021/jp044630p CCC: $30.25
Published on Web 03/01/2005

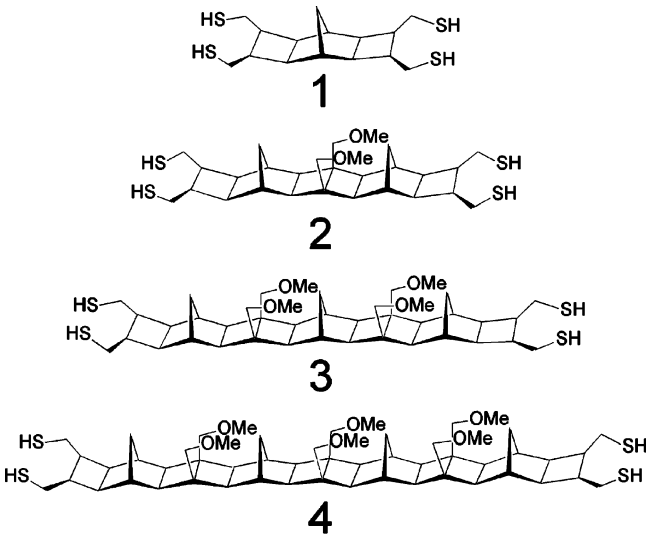

Figure 1. Structures of the norbornylogous molecules **1**−**4**. Due to the synthetic procedures used, each tetrathiol system is, in fact, an equimolar mixture of two diastereomers; see the Supporting Information.

thus complicating the assignment of a transport mechanism. Nevertheless, the monolayer characterization studies indicate that these molecules form reasonably high-quality monolayers. Their ladder-like structure makes them candidates for a wide range of molecular electronics experiments where rigid molecules are desired.

Experimental Section

Fabrication of Au Substrates. Au substrates were fabricated in a manner similar to earlier experiments.[18,28−30,43] Si (100) wafers were coated with 50 Å Cr and 1000 Å Au in a thermal evaporator at a pressure of 1×10^{-6} Torr. The resulting Au surfaces exhibited an RMS roughness of ∼2 nm over an area of 1 μm^2.

Sample Preparation and Storage. Synthetic schemes for the formation of the norbornylogous molecules **1**−**4** (Figure 1) can be found in the Supporting Information. Monolayer films were initially formed in the same manner as alkanethiols—Au substrates were exposed to millimolar solutions of the molecules in CH_2Cl_2 for 12 h. Thicknesses of films deposited in this manner ranged from 20 to 75 Å for **1**, far too thick to be a single molecular layer. The same was true for the other chain lengths—all molecules preferentially assemble into terlayers or tetralayers if left in solution for 12 h, likely due to disulfide formation.[44−48] This multilayering was controlled by moving to a short deposition period followed by a longer soak period. Films were also deposited from less concentrated solutions. Once the deposition parameters were modified in this manner, the molecules reproducibly assembled into single monolayers on Au. The final deposition conditions for SAM formation were that Au substrates were exposed to 10 μM solutions of molecules **1**−**4** for 1 h, after which they were soaked in neat CH_2Cl_2 for 24 h. Samples were stored in CH_2Cl_2 until analysis by spectroscopic ellipsometry, reflection−absorption infrared spectroscopy (RAIRS), Rutherford backscattering spectrometry (RBS), X-ray photoelectron spectroscopy (XPS), or conducting probe-AFM. Upon removal from CH_2Cl_2, the samples were rinsed in neat ethanol or CH_2Cl_2 and blown dry with N_2.

SAM Thickness by Spectroscopic Ellipsometry. Ellipsometric measurements were made using a Sopra ES4G spectroscopic ellipsometer equipped with a xenon light source. The polarization angles (Ψ and Δ) were measured for both bare Au substrates and SAMs over the wavelength range 250−900 nm at an incident angle of 75° from the surface normal. Prior to SAM deposition, the optical constants n and k (the index of refraction and extinction coefficient, respectively) were calculated for each individual Au substrate using instrument software to convert the Ψ and Δ data assuming a bulk solid (i.e., infinite thickness). After SAM deposition, the polarization measurements were repeated with each sample in the same orientation as when the bare Au substrate measurement was taken. Using the new Ψ and Δ values and fixed values for n and k (1.5 and 0, respectively), the instrument software calculated the film thickness. The calculation is based on a parallel layer model of substrate/film/ambient that assumes the film is homogeneous and isotropic. Reported thicknesses represent an average over approximately 10 different film formations.

SAM Thickness and Orientation by XPS. X-ray photoelectron spectra were taken on a Perkin-Elmer Phi 5400 spectrometer with the Mg Kα X-ray (1253.6 eV) from an anode source using a hemispherical analyzer in an ultrahigh vacuum system. Each sample was transferred from the ambient into the UHV chamber through a high vacuum cell. The X-ray anode was operated at 200 W, and the analyzer at a pass energy of 89.45 eV for survey scans and 17.9 eV for high-resolution scans. Thickness calculations from XPS data for thin films can be calculated on the basis of the attenuation of the Au 4f signal from the substrate. This attenuation is given by

$$\frac{I}{I_0} = \exp\left(-\frac{Z}{\lambda \cos\theta}\right) \tag{1}$$

where Z is the film thickness, I and I_0 an average of the intensities of the Au $4f_{5/2}$ and $4f_{7/2}$ peaks after and before monolayer growth, respectively; θ is the angle of photoelectron detection (from surface normal); λ is the effective attenuation length of the photoelectron through the carbon chain. In these experiments, θ was 45° and the effective attenuation length of photoelectrons was taken to be 34.63 Å.[49,50]

In addition to measuring film thicknesses, XPS analysis was also used to determine the binding energies of various sulfur species. In these determinations, high-resolution scans were performed on the S 2p region. Because the binding energies associated with free thiol and bound thiol are so similar, a peak fitting routine was used to deconvolute the two signals. Fits to the data used a combination of Gaussian and Lorentzian line shapes. To fit the S $2p_{3/2,1/2}$ doublet, we used a pair of peaks with the same full width at half-maximum, the standard spin−orbit splitting of 1.17 eV, and a branching ratio of 0.5555 (S $2p_{1/2}$/S $2p_{3/2}$). An oxidized sulfur species with a binding energy of 167.9 eV contributes approximately 10% of the total peak area. We have assumed that the oxidized sulfur peak arises solely from sulfur atoms that are not bound to the metal surface. The XPS system used for analysis is not equipped with an X-ray monochromator, which makes complete peak separation impossible, due to the decreased energy resolution. These two factors combine to make the error in the measurement of peak areas at least 20%.

Infrared Spectroscopy. KBr pellet and RAIRs measurements were performed on a Nicolet Series II Magna-IR System 750 FTIR. RAIRS experiments on SAMs of **1**−**4** used a Harrick-Seagull accessory with the IR beam incident at an 86° angle with respect to the surface normal. A total of 2000 scans were collected at 4 cm^{-1} resolution. KBr pellet spectra were measured at 0.5 cm^{-1} resolution with 100 scans. Molecular concentration in the pellets ranged between 3.0×10^{-3} and 9.0×10^{-3} mol

cm^{-3}. Peak areas were determined by baseline correcting the spectra and fitting the peaks with Lorentzian line shapes.

Rutherford Backscattering Spectrometry. He^+ ions for RBS measurements were generated using a MAS 1700 pelletron tandem ion accelerator (5SDH) equipped with a charge exchange RF plasma source by National Electrostatics Corporation (NEC). The software (HYPRA) and analysis equipment (RBS 400) were provided by Charles Evans & Associates. Ions were accelerated at 2 MeV with a beam current of 10 nA. The solid angle subtended by the backscattered ion detector was 3.6 msr. The detector was placed at a 165° angle with respect to the incident beam on the sample. Silicon (100) substrates for monolayer formation were coated with 400 Å Au without a Cr adhesion layer for an improved RBS signal-to-background ratio. Polar scans were first performed in the silicon region to find the sample orientation that maximized channeling effects. This minimized the background signal from the single-crystal Si substrate (and thus maximized the overall signal-to-noise ratio in the non-Si regions of the spectrum). Charge (200 μC) was then collected in increments of 20 μC at one point on each sample; the total collection time was ~5 h per sample. Data were taken in increments in case film degradation would occur during an extended measurement. Degradation was not observed as determined by a constant sulfur signal across the 10 acquisitions. Molecular surface coverage was determined by dividing the measured sulfur coverage by four, as there are four sulfur atoms per molecule.

Electrical Characterization by CP-AFM. Two distinct types of experiments were performed in this study. One set of experiments was designed to compare transport in the norbornyl homologues with transport in alkanethiols and -dithiols. The AFM tips used for this set of experiments had a nominal radius of 20 nm, and were purchased from Digital Instruments. The coating procedure was the same as described below for large-area tips. The AFM tips used for the bulk of norbornylog resistance measurements were plateau-style tips purchased from Pacific Nanotechnology. Tips and silicon substrates were coated with 50 Å Cr and 1000 Å Au in a thermal evaporator at ~1×10^{-6} Torr base pressure. After use, some Au-coated tips were characterized by scanning electron microscopy (SEM) using a JEOL 6500 field-emission gun SEM operating at 10 kV. Current−voltage measurements were made using a modified MultiMode AFM (Digital Instruments). Junctions were formed by bringing Au-coated AFM tips into contact with SAMs on Au substrates. A Keithley 236 source/measure unit was used to apply a voltage to the AFM tip, and the substrate was grounded through a Keithley 6517 DC ammeter. For a typical data taking session with a single Au-coated tip, several $I-V$ traces per SAM were measured, giving an average resistance value and standard deviation for each molecular chain.

Results and Discussion

Film quality is a critical factor in CP-AFM studies based on SAMs. At the start of this work, it was not clear whether molecules **1**−**4** would form ordered monolayers. A concern was that the bicyclic nature of the bridges forces each chain to possess a large effective cross-section, which could potentially result in disorder because the molecules cannot pack as tightly as in the alkanethiol system. Further, energy minimizations have shown[51] that these rigid molecules exhibit a curved backbone, which should further decrease packing efficiency, as illustrated in Figure 2. Finally, the α,ω-functionalization with thiol groups could allow the molecules to bind to the surface at both ends (hairpin); the probability of such an event increases as the chain length increases. To address these issues, we have extensively characterized the thickness, molecular orientation, and surface coverage of the films using spectroscopic ellipsometry, XPS, RAIRS, and RBS.

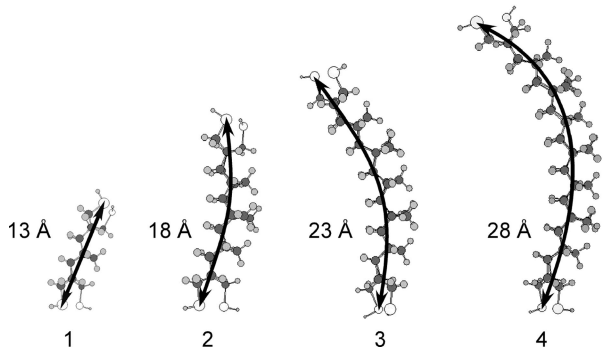

Figure 2. B3LYP/6-31G(d) minimization of structures related to the norbornylogous molecules used in this study. CH_2OCH_3 has been replaced with a methyl group for computational expediency. Also shown is the calculated molecular contour length.

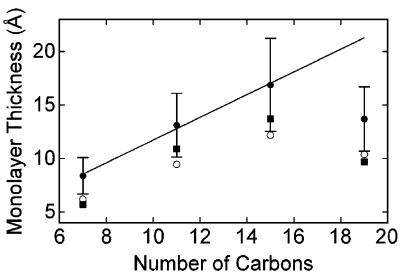

Figure 3. Average of 10−20 thickness measurements obtained by ellipsometry (filled circles) increasing monotonically with molecular contour length for SAMs of **1**−**3**. Extrapolation of this trend shows an 8−9 Å offset between the measured value of film thickness for SAMs of **4** and the expected thickness. Error bars represent one standard deviation from the mean. Also shown are the thicknesses of four individual SAM samples (one sample of each chain length) determined by XPS (open circles) and ellipsometry (filled squares) for a direct comparison of thickness between the two techniques. Good correlation is shown between thickness obtained by XPS and thickness obtained by ellipsometry.

Monolayer Thickness. Film thicknesses for the various chain lengths determined by ellipsometry are shown in Figure 3. The thicknesses of SAMs of **1**−**3** increase linearly with the number of carbons in the chain. One would expect **4** to follow this trend also, because it is a homologue of the previous molecules. However, the thickness of SAMs of **4** is ~8 Å less than predicted by extending the trendline over an additional four carbon atoms. Also shown in Figure 3 are film thicknesses determined by XPS. The XPS results clearly corroborate the ellispometry data, and show again that the thickness of SAMs of **4** is less than the predicted thickness. The discrepancy in the thickness of SAMs of **4** with respect to the measured thicknesses of SAMs of **1**−**3** suggests two possibilities. The first is that the inconsistency in measured thickness represents a decrease in the average tilt angle of molecules in SAMs of **4** with respect to **1**−**3**. The second possibility is that **4** is long enough to hairpin to the surface. To distinguish between a change in tilt angle and a change to a hairpinned structure, we analyzed films by RAIRS, RBS, and XPS.

Monolayer Surface Coverage. Infrared spectra of organic monolayers can be analyzed to obtain a relative packing density and also to determine molecular orientation. We have compared the relative peak areas of the primary methoxy C−O stretch in bulk samples of **1**−**4** to their corresponding values in SAMs.

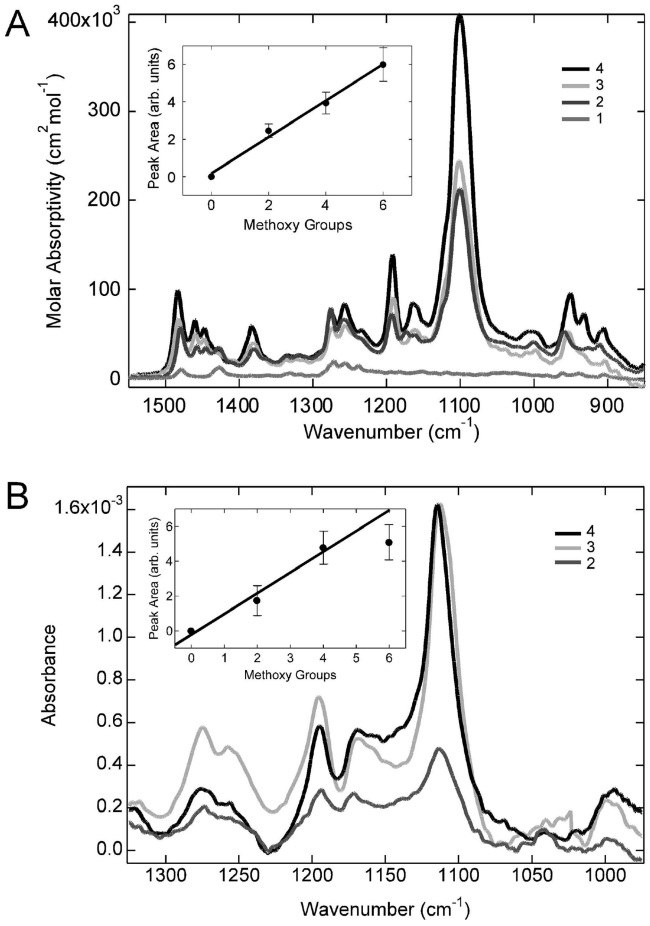

Figure 4. (A) Bulk phase FTIR absorbance spectrum of the norbornylogous molecules in a KBr matrix. The inset shows linear scaling of the C−O stretch at 1114 cm^{-1} with the number of methoxy groups per molecule. (B) RAIRS spectra of **2**−**4** show a nonlinear scaling of the C−O stretch with the number of methoxy groups. The decreased area of **4** supports a decrease in surface coverage.

In the case of the bulk-phase measurements, care was taken to determine the exact amount of sample inserted into the KBr matrix. This allows us to make molar absorptivity measurements of the methoxy absorption. As shown in Figure 4A, the molar absorptivity associated with the methoxy peak at 1114 cm^{-1} in the bulk phase scales linearly with the number of methoxy groups in the molecule. Because the molecules in question form a homologous series, we would expect the same type of scaling in the case of the monolayer spectra if both the surface coverage and molecular orientation remain constant across the series. However, as shown in Figure 4B, there is an obvious difference in the spectrum of SAMs of **4** when compared to SAMs of **1**−**3** − the primary methoxy peak at 1114 cm^{-1} has been damped. The area of this peak is now essentially equal to the peak area associated with SAMs of **3**. This decrease in peak area suggests that there are less methoxy groups (and therefore fewer molecules) on the surface in the case of **4** than there are for SAMs of **1**−**3**, i.e., that the surface coverage of **4** is lower than that of **1**−**3**.

To determine the surface coverage quantitatively, we have used RBS to measure the surface concentration of sulfur atoms. There are only a few literature examples involving RBS analysis of organic monolayers,[52−54] and the focus of those papers is not on determining sulfur content. To our knowledge, we present the first experimental evidence that RBS is an effective technique for measuring the surface coverage of thiol-based SAMs.

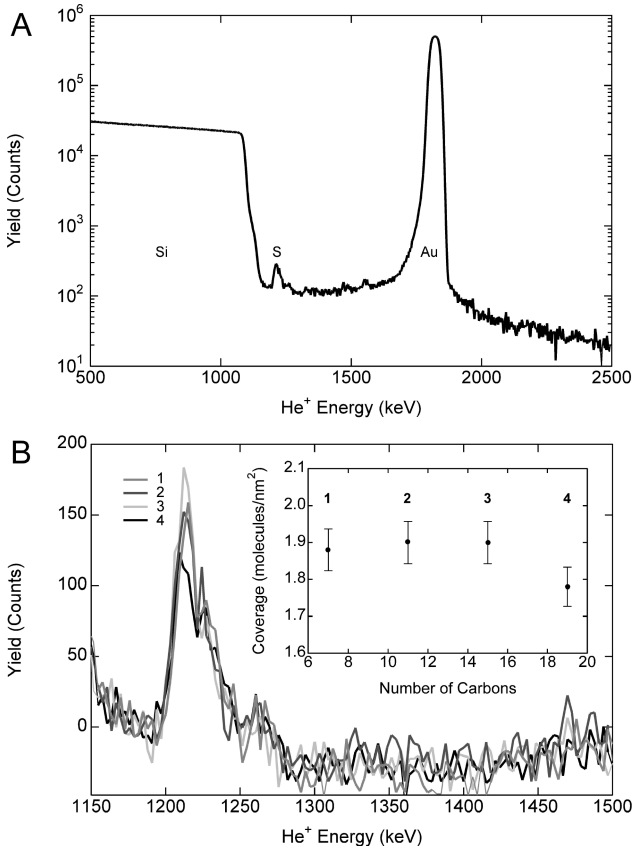

Figure 5. (A) RBS spectrum of **2** on Au-coated silicon wafer. The sulfur peak is easily resolved from both the baseline and the Si peak. (B) RBS spectra of molecules **1**−**4** showing the sulfur region. Baselines have been adjusted to coincide and Gaussian fits were used to determine peak area. The inset shows surface coverage as a function of molecular chain length.

Because there are no published procedures for measuring the sulfur content of SAMs via RBS, it is important to discuss the measurement subtleties involved. Initally, spectra were collected with the incident beam in a random rotation configuration (there is a small amplitude "jitter" on beam position). This configuration is often used to minimize the effects of channeling through the silicon substrate. However, spectra collected in this manner exhibited a sulfur peak that was barely distinguishable from the Si background signal. Changing to fixed position scans resulted in an increase in signal-to-background ratio, making that the preferred method for data collection. As described in the Experimental Section, 10 acquisitions of 20 μC each were added together to improve the signal. Care was also taken to maximize the amount of channeling, which minimizes the contribution of the Si peak in the measured spectrum, and results in a further increase in S/N ratio. Total acquisition time per film was approximately 5 h. A typical spectrum illustrating the relative peak intensities of sulfur and the elements present in the substrate is shown in Figure 5A. An expansion of the sulfur region (Figure 5B) shows a decrease in peak area for SAMs of **4** in relation to SAMs of the other molecules. Peak area (A) is directly related to surface coverage (N_S) through the following equation:

$$N_S = \frac{A}{\sigma \Omega Q} \tag{2}$$

where σ is the average scattering cross section, Ω is the detector solid angle, and Q is the total number of collected He^+ particles. It is clear from Figure 5B that the signal-to-noise ratio is still

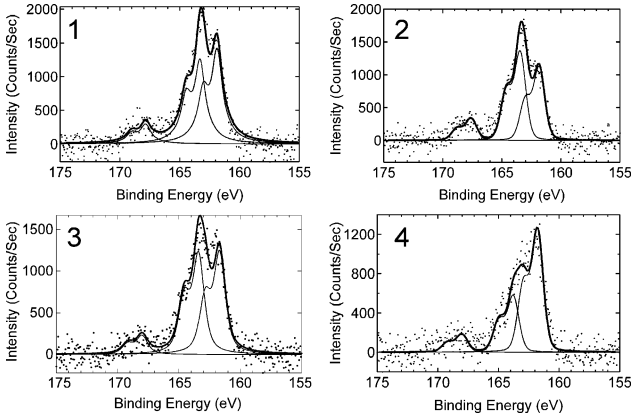

Figure 6. High-resolution XPS scans of the S 2p region in SAMs of **1**−**4** show the presence of three different types of S atoms: bound (∼161.8 eV), unbound (∼163.3 eV), and oxidized (∼167.9), in each SAM. In each scan, the points represent the acquired data, the thin black lines show the contribution to the overall spectrum from each of the sulfur types, and the heavy black line shows the convolved fit spectrum. Note that in SAMs of **1**−**3**, the heights of the peaks corresponding to bound S and unbound S are nearly equivalent; in SAMs of **4**, the bound S peak clearly dominates.

not ideal. For this reason, we fit Gaussians to the sulfur peaks to quantitatively determine the surface coverage of sulfur by determining the peak area of the Gaussian fit. The molecular surface coverage was then calculated by dividing the sulfur coverage by four, as there are four S atoms per molecule. The results of this calculation are shown in the inset in Figure 5B. The data show an essentially constant surface coverage for molecules **1**−**3** (1.88−1.90 molecules/nm^2), and a 6% decrease for **4** (1.78 molecules/nm^2), consistent with the results of ellipsometry and FTIR. Equation 2 does not explicitly account for the roughness of the surface. However, we calculate a surface area of a 1.02 μm^2 for a 1 μm^2 image of a representative Au surface, suggesting that the correction to the surface coverage resulting from the surface roughness is very small.

Film Orientation by XPS. The analyses by FTIR and RBS indicate a smaller surface coverage of **4** with respect to **1**−**3**, but they do not clarify whether this decrease in surface coverage corresponds to a higher degree of molecular tilt with respect to the surface normal or to molecular hairpinning. To address this issue, we have examined the sulfur binding energy (BE) by XPS. XPS has been used extensively in thiol SAM characterization to determine the chemical environment of the sulfur atoms (i.e., whether they are bound to the surface).[55,56] High-resolution scans of the S 2p region are shown in Figure 6. For each of the four SAMs, sulfur exists in three different states: bound (BE ∼ 161.8 eV), unbound (BE ∼ 163.5 eV), and oxidized (BE ∼ 167.8 eV). As stated in the Experimental Section, we employed a peak fitting procedure using Gaussian and Lorentzian line shapes to deconvolute the measured spectra into contributions from the bound and unbound sulfur states. By comparing the area under the bound peak with that of the unbound peak, it is possible to determine whether the molecules are standing up or lying down. Because there are four sulfur atoms per molecule, with two at each end, the area of the bound peak should equal that of the unbound peak if there is no hairpinning to the metal surface. However, the areas that one must compare are not those initially measured, because the electrons emanating from the bound sulfur atoms are attenuated by the carbon backbone of the SAM before reaching the detector. The area under the bound peak must be normalized according to the following equation:

$$A = \frac{A_0}{\exp\left(\frac{-z}{\lambda \cos \theta}\right)} \tag{3}$$

where A and A_0 are the normalized and measured areas of the bound sulfur peak, respectively, and the other variables are defined as in eq 1. In calculating the percent of molecules doubly bound to the surface, we have assumed that the oxidized sulfur peak arises only from sulfur atoms that are not bound to the metal surface. This may not be strictly true, as other groups have shown that surface-bound sulfur atoms do oxidize. However, it is likely that oxidation of the terminal sulfur atoms is more facile than oxidation of the bound atoms, because for oxygen to reach the bound atoms, it must diffuse through the SAM matrix. This leads us to believe that the probability for oxidation of the terminal sulfur atoms is much greater, and so we add the oxidized peak area to the unbound peak area in a calculation of the percentage of hairpinned molecules. Once the normalized areas of bound and unbound peaks are known, the percent of hairpinned molecules can be calculated thusly:

$$\%\ \text{hairpinned} = \frac{\text{area}_{\text{bound}} - (\text{area}_{\text{unbound}} + \text{area}_{\text{oxidized}})}{\text{total peak area}} \tag{4}$$

The results of the above calculation are compiled in Table 1. Because the noise in the XPS spectrum is not ideal, and because we are making the assumption that the oxidized sulfur peak arises totally from the terminal sulfur atoms, we estimate the error in the percentage of hairpinned molecules to be ±20%. On the basis of the linear scaling of the methoxy peak area in FTIR measurements, the linear thickness increase as monitored by ellipsometry and XPS, and the similar surface coverage as determined by RBS, it is likely that SAMs of **1**−**3** have a similar percent of hairpinned molecules (i.e., the different percentages of hairpinned molecules for SAMs of **1**−**3** in Table 1 are not statistically significant). The small amount of hairpinning predicted by XPS analysis coupled with the high degree of error leads us to believe that **1**−**3** form SAMs that are bound to the surface only on one end (i.e., 0% hairpinning). The conclusion that **1**−**3** stand upright is further bolstered by a simple analysis of the chain tilt angle using the ellipsometric data. Using molecular lengths calculated by a B3LYP energy minimization and the average SAM thickness from ellipsometry, we calculate the tilt angles of **1**−**3** to be 39, 34, and 34°, respectively,

TABLE 1: Thicknesses and Sulfur Peak Areas for the Norbornylog SAMs Determined by XPS

		sulfur peak areas				
molecule	XPS thickness (Å)	oxidized	unbound	bound (measured)	bound (normalized)	percent hairpinned[a]
1	6.2	722	3042	3425	4409	8%
2	9.5	633	2601	2149	3162	−1%
3	12.2	512	2686	2709	4455	16%
4	10.4	349	1109	2398	3663	43%

[a] The error associated with this value is ±20% (i.e., the percent of hairpinned molecules in SAMs of **4** ranges from 23 to 63%).

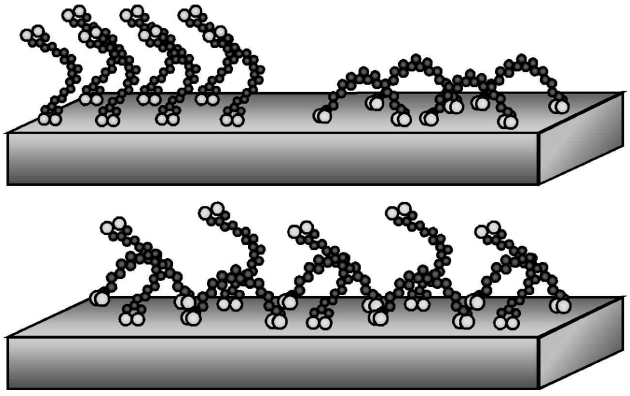

Figure 7. (Top) two possible film orientations for molecules in norbornylog SAMs. Molecules are either bound to the surface at one end, as shown in the left half of the top panel, or they are bound twice (hairpinned), as shown on the right. It is unclear whether mixed-phase SAMs in which some molecules stand up and some are hairpinned exist as phase-separated monolayers (top panel) or as integrated mixtures of standing up and lying down molecules (bottom panel).

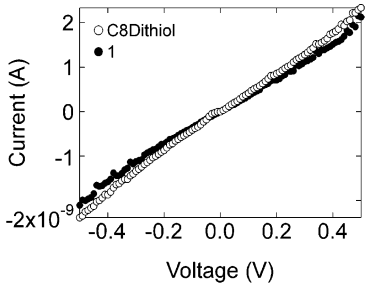

Figure 8. Single AFM tip used to acquire current−voltage data from SAMs of **1** (filled circles) and SAMs of octanedithiol (open circles). The similarity in measured current values between the two molecules suggests that they have similar electronic structures. The fact that the measured current for **1** is on par with that measured for octanedithiol also suggests that the terminal S atoms of **1** make contact with the AFM tip (see text).

assuming no hairpinning in each case. The similarity of the tilt angles suggests that SAMs of **1**−**3** have similar orientation, and no change in the percentage of hairpinned molecules from one SAM to the next. A similar calculation for molecules of **4** gives a tilt angle of 55°. It is obvious from every analysis technique that SAMs of **4** are different from SAMs of **1**−**3**, and we are confident on the basis of the data from ellipsometry, FTIR, RBS, and XPS that SAMs of **4** have some fraction of molecules doubly bound to the substrate metal surface (Figure 7).

Electrical Characterization by CP-AFM. As stated in the Experimental Section, two types of AFM experiments were performed. In the first, we coated a standard pyramidal AFM tip with Au for use as a nanoscale spring-loaded top contact. We brought this electrode into contact with SAMs on Au under 2 nN applied load, and applied a voltage sweep to the tip while the substrate was held at ground. The purpose of this set of measurements was to verify that SAMs of **1**−**4** could indeed be used for CP-AFM experiments, and to compare their current−voltage characteristics with those of a system more familiar to us: alkanedithiol SAMs. Figure 8 shows a comparison between the *I*−*V* behavior of **1** and octanedithiol on Au. Both *I*−*V* curves are linear over a 0.5 V sweep range, and the two molecules have very similar resistance values. Octanedithiol has one more C−C bond along its molecular axis than does **1**, which suggests that it should have a slightly higher resistance that is not reflected in the data in Figure 8. However, due to substrate roughness, there is at least an order of magnitude

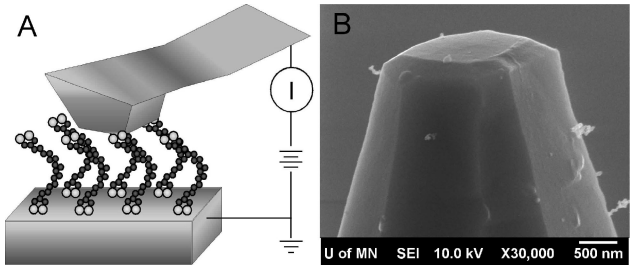

Figure 9. (A) Schematic of the CP-AFM experiment performed with plateau-style AFM tips illustrating the tip−molecule−substrate junction. (B) SEM micrograph of the large-area plateau on the end of the AFM tip.

of variance associated with the trace-to-trace resistance measured for a given tip. On the basis of prior experiments, we would expect only about a factor of 5 lower current for the octanedithiol, which is within the variance of our measurement. Therefore it is not surprising that the *I*−*V* traces of the two molecules are essentially the same. The similarity in measured resistance values suggests that the same transport mechanism occurs through each of the two SAMs. Prior experiments on SAMs with alkyl backbones have shown the dominant transport mechanism to be nonresonant tunneling (assisted by the molecular HOMO).[3] Thus, the transport mechanism in norbornylogs is also likely to be HOMO-mediated tunneling. The similarity of measured currents between **1** and octanedithiol also suggests that the terminal S atoms in norbornylog SAMs are able to form chemical bonds with the AFM tip. This follows because in prior experiments, we have observed 2 orders of magnitude less current in SAMs of molecules terminated by a methyl group than those terminated by a sulfur atom.[29] The CH_3−tip contact is physical in nature, and results in poor orbital overlap between atoms in the tip and atoms in the molecular chain. The S-tip contact is a chemical bond, and results in greatly increased molecule−electrode coupling and therefore decreased contact resistance. If the terminal S atoms in **1** were unavailable for bonding to the tip (i.e., the curved molecular backbone caused the S atoms to become partially buried in the sea of carbon atoms), we would expect *I*−*V* measurements on SAMs of **1** to show greatly reduced current with respect to octanedithiol. Because that is not the case, it appears that SAMs of **1**−**4** form S−Au bonds on both sides of the molecular junction.

The second set of CP-AFM experiments we performed was designed to test the length dependence of conductance in the norbornylog series. In past experiments, we have typically used metal-coated Si_3N_4 contact-mode tips that have a radius of ∼50 nm. However, the longest aliphatic chains we can reliably measure using such tips are on the order of 12 carbon atoms (e.g., dodecanethiol). Voltage sweeps on longer molecules result in currents that are <1 pA, which is below our current sensitivity. Two of the norbornylogous molecules (**3** and **4**) are longer than 12 carbon atoms, which required the use of tips with larger contact areas. We used plateau-style tips from Pacific Nanotechnology that consist of an AFM tip that has been truncated perpendicular to its *z*-axis, resulting in a structure that has a micron-sized plateau used to contact the SAMs as shown in Figure 9. It is not the case that the tip is atomically flat over the entire plateau (i.e., there may be metallized surface particles that make contact to the molecules); however, the resulting contact area is hundreds of times larger than in the case of contacts made with standard AFM tips. Because the number and size of metallized asperities varies from tip to tip, the contact area between tips can vary by orders of magnitude, thus causing

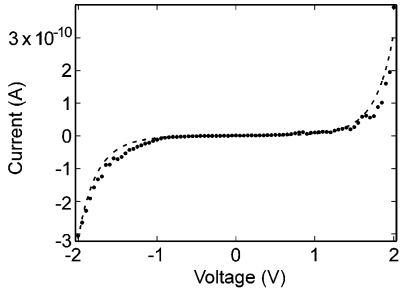

Figure 10. Current−voltage behavior of a CP-AFM junction incorporating **4**. The dashed line is a Simmons fit with parameters: $A = 2.3 \times 10^{-3}$ μm^2, $L = 17.5$ Å, $\varphi = 1.8$ eV.

the current to vary accordingly. For that reason, we have used a single tip to electrically characterize SAMs of **1**−**4**.

Figure 10 shows the sigmoidal dependence of current on voltage for a SAM of **4** on Au. This trace is similar in shape to $I-V$ characteristics observed for SAMs with alkyl backbones. The dashed line is a fit to the Simmons equation for tunneling through a rectangular barrier:[57]

$$I = \frac{qA}{4\pi^2\hbar L^2}\left\{\left(\phi - \frac{qV}{2}\right)\exp\left[-\frac{2\sqrt{2m(\phi - qV)}}{\hbar}L\right] - \left(\phi + \frac{qV}{2}\right)\exp\left[-\frac{2\sqrt{2m(\phi + qV)}}{\hbar}L\right]\right\} \quad (5)$$

where ϕ is the height of the barrier, L is the barrier width, m is the electron mass, and A is the electrode area. The reasonable fit provides qualitative support for nonresonant tunneling as the transport mechanism, though it is well-known that the Simmons model is only a crude approximation for nonresonant tunneling in molecular junctions.[29] Though an exact assignment of the transport mechanism as nonresonant tunneling is impossible without temperature dependent measurements, more evidence for that mechanism is found in Figure 11. Figure 11A shows that over small voltage sweeps, the traces are linear and the slopes clearly decrease with increasing chain length. Figure 11B shows that the current decreases exponentially with chain length as expected for nonresonant tunneling.

The key result of this study is shown in Figure 12, which shows a semilog plot of low voltage resistance versus molecular contour length (number of carbons) for SAMs of **1**−**4**. In the low-voltage regime, the characteristic equation for nonresonant tunneling is

$$R = R_0 \exp(\beta s) \quad (6)$$

where R is the junction resistance, R_0 is the contact resistance, β is the tunneling attenuation factor, and s is the junction length. Resistance values plotted in Figure 12 were obtained from linear fits to several low-voltage $I-V$ curves of each molecule, which generated a resistance and standard deviation for each chain length. There is a clear exponential dependence of resistance on chain length for all molecules. This is consistent with eq 6 for nonresonant tunneling. From the slope of the graph in Figure 12 we extract a value of 1.1 C^{-1} (0.9 Å^{-1}) for β. The β value is in excellent agreement with β values determined for saturated alkane chains in molecular junctions. The similarity of β values between the norbornyl and alkyl systems suggests that the electronic details of molecular junctions formed from SAMs of each type of molecule (i.e., charge transfer at the metal−molecule interface, relative position of the molecular energy levels with respect to the system Fermi level, etc.) are also similar.

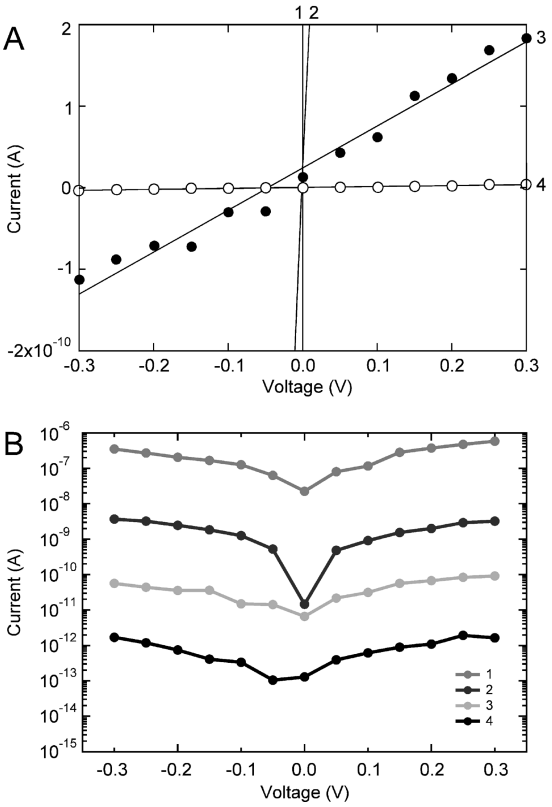

Figure 11. (A) Measured currents for **1**−**4** are linear over the low-voltage regime, and currents decrease with increasing chain length. (B) Current scales exponentially with chain length, consistent with a nonresonant tunneling mechanism.

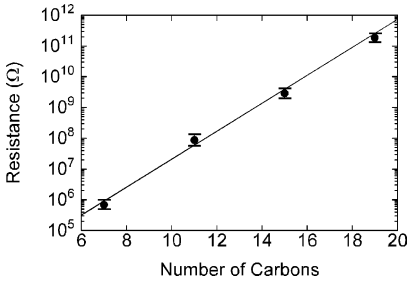

Figure 12. Semilog plot of resistance versus molecular length for junctions based on SAMs of **1**−**4**. Although the SAM thickness does not increase monotonically with chain length, the resistance scales exponentially with the number of carbon atoms in the chain.

Note that it is perhaps surprising that the data in Figure 12 nicely fit eq 6. For example, one might have expected that the resistance would scale exponentially with SAM thickness instead of molecular contour length (i.e., a through-space transport mechanism instead of through-bond). However, it is important to keep in mind that the apparent thickness of SAMs of **4** is the result of averaging over domains of upright and hairpinned molecules. Assuming 43% of the molecules in SAMs of **4** are hairpinned, and a 36° tilt angle for the nonhairpinned molecules, we predict a thickness of 8 Å for hairpinned molecules and a thickness of 19 Å for nonhairpinned molecules. Thus it is possible that the tip only contacts the molecules that are singly bound because they are more than twice as tall as the doubly bound molecules. In this scenario, substitution of a junction length of 19 Å, a contact resistance of 6000 Ω, and a β value of 0.9 Å^{-1} into eq 6 gives a theoretical junction resistance of 2×10^{11} Ω, exactly the measured resistance of the junction. This suggests that it is definitely possible for the AFM tip to be contacting only the molecules that stand up in mixed-phase

SAMs, and therefore it is reasonable for the junction resistance to scale with the contour length of the molecules in Figure 12.

Conversely, if the tip could make contact with hairpinned molecules, the contact point would be somewhere in the middle of the molecular backbone. This has two consequences: there is likely now a tip−methylene contact instead of a tip−sulfur contact, and the probable tunneling distance is half what it would be for an upright molecule. Prior experiments in our laboratories have shown a factor of 100 increase in resistance for metal−CH_3 contacts compared to metal−S contacts. However, that small increase pales in comparison to the decreased resistance that would arise from a drastic decrease in the length of the tunneling junction. Using the thickness values calculated earlier, and a contact resistance of 600 000 Ω, we calculate the junction resistance to be 1×10^9 Ω for the scenario where the tip contacts both hairpinned and nonhairpinned molecules.[58] This is 2 orders of magnitude less than the measured resistance, and thus it is unlikely that the tip is contacting both hairpinned and nonhairpinned molecules simultaneously.

Conclusions

We have synthesized a series of thiol-terminated norbornylogs and formed SAMs of them on Au from CH_2Cl_2. SAMs were characterized structurally using ellipsometry, FTIR, RBS, and XPS, and electrically with CP-AFM. Structural characterization shows that **1**−**3** form similarly oriented monolayers, bound to the Au surface only on one end, with an average tilt angle of 36° with respect to the surface normal. Molecules of **4** form SAMs with a structure different from those of **1**−**3**, in which a fair percentage of molecules are bound to the Au substrate at both ends. By using large-area AFM tips to make $I-V$ measurements, we have probed conductance through norbornylogs **1**−**4**, which range from 13 to 28 Å in length. Electrical characterization shows strong evidence for a charge transport mechanism of nonresonant tunneling, as determined by the exponential dependence of resistance on molecular length. Although SAMs of **4** contain some hairpinned molecules, our results show that the resistance of junctions of SAMs of **4** scales as if there were no hairpinned molecules, likely because the tip does not make contact with molecules that are not standing up.

Acknowledgment. J.M.B. thanks John C. Nelson of the University of Minnesota Characterization Facility and Yongqiang Wang now with Los Alamos National Labs for assistance with spectroscopic ellipsometry and RBS measurements, respectively. C.D.F. thanks the National Science Foundation (DMR-0084404, CHE-0315165) for financial support. The Australian group thanks the Australian Research Council for support, and the Australian Partnership for Advanced and the Computing (APAC) and the Australian Centre for Advanced Computing and Communications (AC3) for allocation of computing time.

Supporting Information Available: Experimental details for the synthesis of compounds **1**−**4**. This information in available free of charge at http://pubs.acs.org.

References and Notes

(1) Reichert, J.; Weber, H. B.; Mayor, M.; von Lohneysen, H. *Appl. Phys. Lett.* **2003**, *82*, 4137−4139.

(2) Kergueris, C.; Bourgoin, J. P.; Palacin, S.; Esteve, D.; Urbina, C.; Magoga, M.; Joachim, C. *Phys. Rev. B* **1999**, *59*, 12505−12513.

(3) Wang, W.; Lee, T.; Reed, M. A. *Phys. Rev. B* **2003**, *68*, 035416/1−035416/7.

(4) Wang, W.; Lee, T.; Kretzschmar, I.; Reed, M. A. *Nano Lett.* **2004**, *4*, 643−646.

(5) Kushmerick, J. G.; Lazorcik, J.; Patterson, C. H.; Shashidhar, R.; Seferos, D. S.; Bazan, G. C. *Nano Lett.* **2004**, *4*, 639−642.

(6) Pollack, S. K.; Naciri, J.; Mastrangelo, J.; Patterson, C. H.; Torres, J.; Moore, M.; Shashidhar, R.; Kushmerick, J. G. *Langmuir* **2004**, *20*, 1838−1842.

(7) Chabinyc, M. L.; Chen, X.; Holmlin, R. E.; Jacobs, H.; Skulason, H.; Frisbie, C. D.; Mujica, V.; Ratner, M. A.; Rampi, M. A.; Whitesides, G. M. *J. Am. Chem. Soc.* **2002**, *124*, 11730−11736.

(8) Liu, Y.-J.; Yu, H.-Z. *ChemPhysChem* **2003**, *4*, 335−342.

(9) Solak, A. O.; Ranganathan, S.; Itoh, T.; McCreery, R. L. *Electrochem. Solid-State Lett.* **2002**, *5*, E43-E46.

(10) Slowinski, K.; Slowinska, K. U.; Majda, M. *J. Phys. Chem. B* **1999**, *103*, 8544−8551.

(11) Bumm, L. A.; Arnold, J. J.; Dunbar, T. D.; Allara, D. L.; Weiss, P. S. *J. Phys. Chem. B* **1999**, *103*, 8122−8127.

(12) Bumm, L. A.; Arnold, J. J.; Cygan, M. T.; Dunbar, T. D.; Burgin, T. P.; Jones, L., II.; Allara, D. L.; Tour, J. M.; Weiss, P. S. *Science* **1996**, *271*, 1705−07.

(13) Ishida, T.; Mizutani, W.; Choi, N.; Akiba, U.; Fujihira, M.; Tokumoto, H. *J. Phys. Chem. B* **2000**, *104*, 11680−11688.

(14) Guisinger, N. P.; Greene, M. E.; Basu, R.; Baluch, A. S.; Hersam, M. C. *Nano Lett.* **2004**, *4*, 55−59.

(15) Datta, S.; Tian, W.; Hong, S.; Reifenberger, R.; Henderson, J. I.; Kubiak, C. P. *Phys. Rev. Lett.* **1997**, *79*, 2530−2533.

(16) Gomar-Nadal, E.; Ramachandran, G. K.; Chen, F.; Burgin, T.; Rovira, C.; Amabilino, D. B.; Lindsay, S. M. *J. Phys. Chem. B* **2004**, *108*, 7213−7218.

(17) Ishida, T.; Mizutani, W.; Liang, T.-T.; Azehara, H.; Miyake, K.; Sasaki, S.; Tokumoto, H. *Ann. N. Y. Acad. Sci.* **2003**, *1006*, 164−186.

(18) Wold, D. J.; Haag, R.; Rampi, M. A.; Frisbie, C. D. *J. Phys. Chem. B* **2002**, *106*, 2813−2816.

(19) Cui, X. D.; Primak, A.; Zarate, X.; Tomfohr, J.; Sankey, O. F.; Moore, A. L.; Moore, T. A.; Gust, D.; Nagahara, L. A.; Lindsay, S. M. *J. Phys. Chem. B* **2002**, *106*, 8609−8614.

(20) Cui, X. D.; Primak, A.; Zarate, X.; Tomfohr, J.; Sankey, O. F.; Moore, A. L.; Moore, T. A.; Gust, D.; Harris, G.; Lindsay, S. M. *Science* **2001**, *294*, 571−574.

(21) Le, J. D.; He, Y.; Hoye, T. R.; Mead, C. C.; Kiehl, R. A. *Appl. Phys. Lett.* **2003**, *83*, 5518−5520.

(22) Chen, J.; Wang, W.; Reed, M. A.; Rawlett, A. M.; Price, D. W.; Tour, J. M. *Appl. Phys. Lett.* **2000**, *77*, 1224−1226.

(23) Metzger, R. M. *Chem. Rev.* **2003**, *103*, 3803−3834.

(24) Xu, B.; Zhang, P.; Li, X.; Tao, N. *Nano Lett.* **2004**, *4*, 1105−1108.

(25) Xiao, X.; Xu, B.; Tao, N. J. *Nano Lett.* **2004**, *4*, 267−271.

(26) Luo, Y.; Collier, C. P.; Jeppesen, J. O.; Nielsen, K. A.; Delonno, E.; Ho, G.; Perkins, J.; Tseng, H.-R.; Yamamoto, T.; Stoddart, J. F.; Heath, J. R. *ChemPhysChem* **2002**, *3*, 519−525.

(27) Lau, C. N.; Stewart, D. R.; Williams, R. S.; Bockrath, M. *Nano Lett.* **2004**, *4*, 569−572.

(28) Wold, D. J.; Frisbie, C. D. *J. Am. Chem. Soc.* **2000**, *122*, 2970−2971.

(29) Engelkes, V. B.; Beebe, J. M.; Frisbie, C. D. *J. Am. Chem. Soc.* **2004**, *126*, 14287−14296.

(30) Beebe, J. M.; Engelkes, V. B.; Miller, L. L.; Frisbie, C. D. *J. Am. Chem. Soc.* **2002**, *124*, 11268−11269.

(31) Tong, G. S. M.; Kurnikov, I. V.; Beratan, D. N. *J. Phys. Chem. B* **2002**, *106*, 2381−2392.

(32) Winkler, J. R.; Di Bilio, A. J.; Farrow, N. A.; Richards, J. H.; Gray, H. B. *Pure Appl. Chem.* **1999**, *71*, 1753−1764.

(33) Goldman, C. *Phys. Rev. A: Ato., Mol., Opt. Phys.* **1991**, *43*, 4500−9.

(34) Jones, M. L.; Kurnikov, I. V.; Beratan, D. N. *J. Phys. Chem. A* **2002**, *106*, 2002−2006.

(35) Kelley, S. O.; Barton, J. K. *Science* **1999**, *283*, 375−381.

(36) Arkin, M. R.; Stemp, E. D. A.; Holmlin, R. E.; Barton, J. K.; Hormann, A.; Olson, E. J. C.; Barbara, P. F. *Science* **1996**, *273*, 475−480.

(37) Seischab, M.; Lodenkemper, T.; Stockmann, A.; Schneider, S.; Koeberg, M.; Roest, M. R.; Verhoeven, J. W.; Lawson, J. M.; Paddon-Row, M. N. *Phys. Chem. Chem. Phys.* **2000**, *2*, 1889−1897.

(38) Paddon-Row, M. N.; Verhoeven, J. W. *New J. Chem.* **1991**, *15*, 107−16.

(39) Oevering, H.; Paddon-Row, M. N.; Heppener, M.; Oliver, A. M.; Cotsaris, E.; Verhoeven, J. W.; Hush, N. S. *J. Am. Chem. Soc.* **1987**, *109*, 3258−69.

(40) Balaji, V.; Ng, L.; Jordan, K. D.; Paddon-Row, M. N.; Patney, H. K. *J. Am. Chem. Soc.* **1987**, *109*, 6957−69.

(41) Warman, J. M.; De Haas, M. P.; Paddon-Row, M. N.; Cotsaris, E.; Hush, N. S.; Oevering, H.; Verhoeven, J. W. *Nature* **1986**, *320*, 615−16.

(42) Hush, N. S.; Paddon-Row, M. N.; Cotsaris, E.; Oevering, H.; Verhoeven, J. W.; Heppener, M. *Chem. Phys. Lett.* **1985**, *117*, 8−11.

(43) Wold, D. J.; Frisbie, C. D. *J. Am. Chem. Soc.* **2001**, *123*, 5549−5556.
(44) Raymo, F. M.; Alvarado, R. J.; Pacsial, E. J.; Alexander, D. *J. Phys. Chem. B* **2004**, *108*, 8622−8625.
(45) Weckenmann, U.; Mittler, S.; Naumann, K.; Fischer, R. A. *Langmuir* **2002**, *18*, 5479−5486.
(46) Brower, T. L.; Garno, J. C.; Ulman, A.; Liu, G.-y.; Yan, C.; Goelzhaeuser, A.; Grunze, M. *Langmuir* **2002**, *18*, 6207−6216.
(47) Joo, S. W.; Han, S. W.; Kim, K. *Langmuir* **2000**, *16*, 5391−5396.
(48) Kohli, P.; Taylor, K. K.; Harris, J. J.; Blanchard, G. J. *J. Am. Chem. Soc.* **1998**, *120*, 11962−11968.
(49) Laibinis, P. E.; Bain, C. D.; Whitesides, G. M. *J. Phys. Chem.* **1991**, *95*, 7017−21.
(50) Bain, C. D.; Whitesides, G. M. *J. Phys. Chem.* **1989**, *93*, 1670−3.
(51) Unconstrained geometry optimizations were carried out at the B3LYP/6-31G(d) level of theory, using Gaussian 98, Revision A.7; Gaussian, Inc: Pittsburgh, PA.
(52) Wohlfart, P.; Weiss, J.; Kashammer, J.; Winter, C.; Scheumann, V.; Fischer, R. A.; Mittler-Nehera, S. *Thin Solid Films* **1999**, *340*, 274−279.
(53) Winter, C.; Kashammer, J.; Mittle-Neher, S.; Fischer, R. A. *Opt. Mater. (Amsterdam)* **1998**, *9*, 352−355.
(54) Colvin, V. L.; Goldstein, A. N.; Alivisatos, A. P. *J. Am. Chem. Soc.* **1992**, *114*, 5221−30.
(55) Deng, W.; Yang, L.; Fujita, D.; Nejoh, H.; Bai, C. *Appl. Phys. A-Mater.* **2000**, *71*, 639−642.
(56) Rieley, H.; Kendall, G. K.; Zemicael, F. W.; Smith, T. L.; Yang, S. *Langmuir* **1998**, *14*, 5147−5153.
(57) Simmons, J. G. *J. Appl. Phys.* **1963**, *34*, 1793−1803.
(58) The contact resistance associated with the tip−norbornylog−substrate junction was 6000 Ω. Under the assumption that contacting the backbone of hairpinned molecules is similar to making contact with a CH_3 group, we expect a contact resistance approximately 100 times greater than in the case of the norbornylogs.